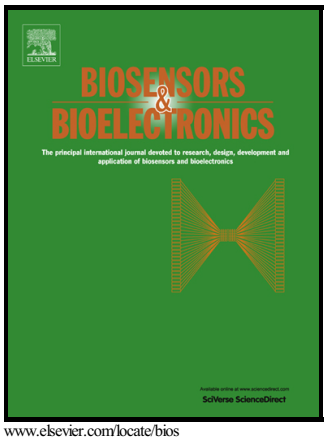

www.elsevier.com/locate/bios

2D and 3D graphene materials: Preparation and bioelectrochemical applications

Hongcai Gao, Hongwei Duan

PII: S0956-5663(14)00866-5
DOI: http://dx.doi.org/10.1016/j.bios.2014.10.067
Reference: BIOS7251

To appear in: *Biosensors and Bioelectronic*

Received date: 21 August 2014
Revised date: 27 October 2014
Accepted date: 29 October 2014

Cite this article as: Hongcai Gao and Hongwei Duan, 2D and 3D graphene materials: Preparation and bioelectrochemical applications, *Biosensors and Bioelectronic,* http://dx.doi.org/10.1016/j.bios.2014.10.067

2D and 3D graphene materials: Preparation and bioelectrochemical applications

Hongcai Gao, Hongwei Duan*

School of Chemical and Biomedical Engineering, Nanyang Technological University, 70 Nanyang Drive, Singapore, 637457

* Corresponding author at: School of Chemical and Biomedical Engineering, Nanyang Technological University, 70 Nanyang Drive, Singapore 637457, Tel.: +65 6514 1019; E-mail address: hduan@ntu.edu.sg

Abstract:

The attractive properties of graphene materials have stimulated intense research and development in the field of bioelectrochemistry. In particular, the construction of 2D and 3D graphene architectures provides new possibilities for developing flexible and porous carbon scaffolds, which not only inherit some of the key properties of individual graphene sheets, but also develop additional functions that are of considerable interest for bioelectrochemical applications. In this review article, we will first summarize the recently developed approaches to preparing graphene sheets, and then focus on the methods to assemble them into macroscopic 2D and 3D structures. Furthermore, we will highlight the potential applications of these materials in electrochemical biosensors and biological fuel cells.

Keywords:

Graphene paper, Graphene hydrogel, Graphene foam, Biosensor, Biological fuel cell

1. Introduction

The successful isolation of high quality graphene with the size of hundreds of microns from graphite in 2004 (Novoselov et al., 2004) aroused tremendous efforts towards investigating the unique properties, controlling the growth, introducing diverse functionalities, and eventually exploring the potential applications of graphene materials (Novoselov et al., 2012; Qian et al., 2011a; Zhu et al., 2010b). In particular, graphene derivatives have been actively studied in the field of electrochemistry because of their unique physicochemical properties in comparison with other carbon materials. the, graphene exhibits a unique combination of physical and chemical properties such as large specific surface area (2630 m^2 g^{-1}) (Stoller et al., 2008), superior electrical conductivity (200 S m^{-1}) (Stankovich et al., 2007; Yoo et al., 2011), excellent thermal stability with oxidation resistance temperature up to 601 °C (Wu et al., 2009b), high thermal conductivity between 3080 to 5150 W m^{-1} K^{-1} (Ghosh et al., 2008), remarkable mechanical strength with Young's modulus of around 1.0 TPa (Lee et al., 2008), and outstanding optical transmittance of 97.7% (Nair et al., 2008). Moreover, it also shows fascinating electrochemical properties, including wide electrochemical potential windows, low charge-transfer resistance, and excellent electrochemical activity (Chen et al., 2014; Qian et al., 2011b; Shao et al., 2010b). The aforementioned physical and electrochemical properties enable the widespread use of graphene in the field of bioelectrochemistry, and possibly offer new solutions to address the current energy and healthcare issues that are of great importance for the sustainable development of the society.

Chemically derived graphene, including graphene oxide (GO) and reduced graphene oxide (rGO), are promising building blocks to construct 2D and 3D materials (Bi et al., 2012; Cheng and Li, 2013). In addition to the inherent properties of individual graphene sheets, versatile

functionalities can be built in the hierarchical graphene materials for improved performance (Chen et al., 2013; Ren and Cheng, 2013). In comparison with the extensive research on individual graphene sheets, less attention has been focused on 2D and 3D graphene materials. One of the goals of this review is to increase the visibility of the new class of hierarchical materials and call attention for further research from academia and industry. From a practical point of view, the use of these materials into practical applications relies on the development of efficient preparation procedures that allow for tailoring their structures and functions for improved performance. We will first summarize the approaches for preparing chemically derived graphene, with particular focuses on the recently developed environmentally-friendly methods, and then summarize the strategies to assemble individual graphene sheets into 2D and 3D structures. Their bioelectrochemical applications will be discussed afterwards with an emphasis on the specific topics of electrochemical biosensors and biological fuel cells.

2. Preparation of graphene sheets

Although the scotch-tape method can directly produce high-quality graphene, it is lack of the feasibility of functionalization and not suitable for large-scale production. A diverse range of approaches, therefore, have been developed to produce graphene, including epitaxial growth (Sutter et al., 2008), chemical vapor deposition (CVD) (Mattevi et al., 2011), liquid-phase exfoliation (Hernandez et al., 2008), chemical exfoliation (Dreyer et al., 2010), and organic synthesis (Wu et al., 2007). Among these methods, chemical exfoliation has attracted widespread interest because it does not rely on special equipments and allows for scaled-up preparation of GO carrying a high density of functional groups, which open the possibility to introduce additional functionalities (Park and Ruoff, 2009). This route is referred as oxidation-exfoliation-reduction process, which generally involves chemical oxidation of graphite into graphite oxide,

followed by exfoliation of graphite oxide into single-layered GO, and reduction of GO to rGO with low oxygen to carbon atomic ratio (Fig. 1) (Bai et al., 2011).

(Figure 1 is here)

2.1. Preparation of GO

The precursor of GO is graphite oxide which contains oxygen functionalities and retains stacked structure similar to that of graphite. The history for preparing graphite oxide can be traced back to 1859, when $KClO_3$ and fuming HNO_3 were used to oxidize graphite powder, leading to a material with carbon to oxygen ratio around 2:1 (Brodie, 1859). The utilization of $KClO_3$ and HNO_3 must be handled with special caution because of the generation of highly toxic ClO_2 gas and the possible production of explosion (Compton and Nguyen, 2010). Hummers et al. developed an approach to synthesize graphite oxide with similar level of oxidation but employing different oxidation reagents ($NaNO_3$, $KMnO_4$, and concentrated H_2SO_4) in 1958 (Hummers and Offeman, 1958). Through Hummers' method, the reaction can be completed within relatively shorter reaction time while avoiding the generation of hazardous ClO_2 gas. A recent study revealed that the amount of basal plane in graphite oxide can be improved by eliminating $NaNO_3$, increasing the amount of $KMnO_4$, and performing the reaction in a 9:1 mixture of H_2SO_4 and H_3PO_4 (Marcano et al., 2010). The exfoliation of graphite oxide into single-layered GO can be achieved by employing additional energy inputs, e.g., mechanical shaking or ultrasonication (Li et al., 2008a). Several parameters, including starting materials, oxidation procedures, and the forms of exfoliation energy, play important roles in controlling the size or number of layers of GO. With increasing oxidation time or the amount of oxidants, the average size of GO can be tuned from ~59,000 to ~550 nm^2 (Zhang et al., 2009). Ultrasonication is more effective to reduce the size of GO than mechanical shaking (Pan and Aksay, 2011). The

number of layers of GO in the final products is strongly dependent on the lateral size and crystallinity of graphite precursors (Wu et al., 2009a).

2.2. Reduction of GO

2.2.1. Chemical reduction

The oxidation of graphite by strong oxidants leads to disruption of the sp^2 bonding networks, and therefore the oxidation products, both graphite oxide and GO, are electrically insulating materials. A reduction process is necessitated to remove oxygen functionalities (epoxy, carboxyl, and hydroxyl groups), and recover electrical conductivity by restoring the π-network (Chen et al., 2012a). The advantage of chemical reduction is that it can be carried out at relatively low temperature or with only moderate heating. Importantly, it also does not rely on sophisticate equipments.

Hydrazine is the most efficient reducing reagent to remove oxygen functionalities from GO, leading to rGO with a carbon to oxygen atomic ratio of around 7 and electrical conductivity of ~7200 S m^{-1} (Li et al., 2008a). The successful reduction of GO was also achieved by using freshly-prepared solution of $NaBH_4$ (Gao et al., 2009). In comparison with hydrazine, fewer heteroatoms were introduced when $NaBH_4$ as reducing reagent. Nevertheless, alcohol groups on GO cannot be efficiently removed by $NaBH_4$ because of its low activity for reduction of epoxy and carboxyl groups. In order to avoid the utilization of toxic hydrazine and $NaBH_4$, a number of environmentally-benign reagents have been actively explored, including hydrogen iodide (Pei et al., 2010), ascorbic acid (Zhang et al., 2010), alkaline solution (Park et al., 2008), glutathione (Pham et al., 2011), urea (Lei et al., 2012), amino acids (Chen et al., 2011a), dopamine (Xu et al., 2010a), metal powders (Fan et al., 2010a; Fan et al., 2010b; Mei et al., 2012), low-valence metal

ions (Xue et al., 2011), reducing sugar (Zhu et al., 2010a), tea water (Wang et al., 2011c), and carrot root (Kuila et al., 2012). Among them, ascorbic acid is accepted as an ideal substitute for hydrazine and $NaBH_4$ because of its non-toxicity, remarkable stability in water, and high deoxygenation efficiency. The atomic ratio of carbon to oxygen in rGO reduced by ascorbic acid is comparable to that reduced by hydrazine (Fernandez-Merino et al., 2010).

2.2.2. Electrochemical reduction

Electrochemical reduction is typically achieved by applying a negative potential to GO films coated on conductive substrates. This strategy has several advantages in comparison with chemical reduction (Low et al., 2013; Ramesha and Sampath, 2009; Zhou et al., 2009a). First, electrons work as intrinsically environmentally-friendly reducing reagent, leading to the formation of rGO without heteroatoms contaminations. Furthermore, highly negative potentials, readily obtainable by adjusting electrochemical parameters, are beneficial for removing more oxygen functionalities in the production of high quality rGO. At last, the resulting rGO is in good contact with electrically conductive substrates, which simplifies the electrode fabrication process and is suitable for further electrochemical applications (Shao et al., 2010a).

Cathodic deposition has been widely employed to prepare metal nanoparticles. Thus, electrochemical reduction also opens the way to prepare nanoparticles modified rGO through one-step manner (Zhu et al., 2011a). The prepared nanoparticles were directly immobilized on the surface of rGO without any linker molecules, facilitating electron transfers between the two components. In addition, the abundant oxygen functionalities on GO provide more anchoring sites for metal ions than rGO, and consequently, the density of metal nanoparticles from one-step electrochemical reduction procedure are higher than that from two-step method involving

chemical reduction of GO followed by electrochemical deposition of metal nanoparticles (Fig. 2) (Gao et al., 2011).

(Figure 2 is here)

2.2.3. Hydrothermal or solvothermal reduction

It is also possible to remove oxygen functional groups on GO in pure aqueous or organic solvents under hydrothermal or solvothermal conditions. Protons can be generated from water under hydrothermal conditions, and the mechanism for hydrothermal reduction of GO is considered similar to proton catalyzed dehydration of alcohols (Zhou et al., 2009b). Because of the reversible properties of proton catalyzed dehydration and hydration reactions, there should always be some residual oxygen functionalities on rGO even at the end of reactions. In solvothermal conditions, the temperature required for reduction of GO decreases as the reducing power of organic solvent increases. The minimum temperatures for GO reduction varied from 120 to 160 °C when the solvents changed from glycol to 1-butanol (Nethravathi and Rajamathi, 2008).

Heteroatoms can be introduced into graphene by adding compounds containing the required heteroatoms into GO dispersion under hydrothermal or solvothermal conditions. For example, nitrogen doped graphene has been prepared when hydrazine was used as doping reagents in both water (Long et al., 2010) and N,N-dimethylformamide (Wang et al., 2013b). Hydrothermal or solvothermal method is also facile to prepare a diverse range of nanomaterials, allowing for one-pot or one-step synthesis of graphene-based nanocomposites if the growth of nanomaterials and reduction of GO occur simultaneously. Various metal oxide and sulfides, including Co_3O_4 (Liang et al., 2011), Mn_3O_4 (Wang et al., 2010b), TiO_2 (Shah et al., 2012), MoS_2 (Li et al., 2011a), CdS

and ZnS (Wang et al., 2010c), have been loaded on graphene by heating reaction mixtures containing GO and desired metal ion precursors under hydrothermal or solvothermal conditions. However, the one-step strategy lacks the ability to precisely control the size and distribution of nanoparticles on graphene.

2.2.4. Thermal reduction

The successful exfoliation of single-layer graphene relies on sufficient oxidation of graphite and adequate pressure during direct thermal treatment process (Schniepp et al., 2006). Therefore, special equipments are generally necessitated to obtain rapid heating rates (typically 2000 °C min^{-1}), high temperatures (800-1000 °C), and inert atmospheres (high vacuum, argon or hydrogen gas) (Wang et al., 2012). A number of products can be generated as a result of rapid temperature increase, including CO_2, CO, water, and other small hydrocarbon molecules (Jimenez, 1987; Matuyama, 1954). The generated gases at high temperatures create a huge pressure increase between the stacked layers, and eventually result in exfoliation of stacked platelets (McAllister et al., 2007).

Microwave and photo irradiation represent two kinds of innovative heating sources that can be applied for GO reduction. Compared with traditional thermal methods, uniform and rapid heating can be generated by microwave irradiation within a short time at ambient conditions (Zhu et al., 2010c). The microwave heating can also promote chemical reactions by lowering activation energies and shortening reaction time. Metal nanoparticles decorated graphene have been prepared in one-step manner upon microwave heating the mixture of GO and metal ion precursors. In contrast to the composites prepared by mixing metal nanoparticles and graphene, the one-step procedure produces metal nanoparticles with smaller size and higher density on

graphene (Hassan et al., 2009). It is still challenging to reduce GO incorporated into materials with poor thermal conductivity, such as polymers, which may prevent reducing reagents from completely reducing GO. Photothermal reduction can overcome these shortcomings. A camera flash can provide 9 times of thermal energy needed for heating GO above 100 °C, which is more than sufficient to initiate the thermal deoxygenation of GO (Cote et al., 2009a; Kim et al., 2010a). In addition, photothermal method also enables patterning of GO or GO/polymer films by flashing through photomask, and precisely controls the size, position and shape of the films (Krishnan et al., 2012).

2.2.5. Photo-catalyzed reduction

Inorganic photocatalysts, including semiconductors (ZnO and TiO_2) (Williams and Kamat, 2009; Williams et al., 2008) (Fig. 3) and plasmonic metal nanoparticles (Ag nanoparticles) (Wu et al., 2011), have been successfully applied in light-assisted reduction of GO, when photoexited electrons were injected from semiconductors or metal nanoparticles into conduction band of GO. However, the inorganic nanomaterials cannot be easily removed from the dispersions containing rGO, potentially affecting the properties and limiting the applications of the resulting materials. The development of organic photocatalysts is a promising way to tackle these problems. Clean rGO sheets were prepared with organic photocatalyst, i.e., Hantzsch 1,4-dihydropyridine (HEH), under UV irradiations. HEH and its aromatic pyridine products were easily removed by extraction with ethyl acetate. The resulting rGO exhibits comparable electrical conductivity to that by hydrazine reduction (Zhang et al., 2012).

(Figure 3 is here)

2.2.6. Microbial reduction

Microbial technology was first achieved for reduction of GO in strictly anaerobic environments (Salas et al., 2010). However, a follow-up work revealed that anaerobic condition is not necessary for the microbial reduction to proceed (Wang et al., 2011a). In these two works, GO was reduced by a dissimilatory metal-reducing bacteria, i.e., *Shewanella*, which generate electrons in metabolic process. The generated electrons are transferrable by anaerobic respiration of cells from the cell interior to electron acceptors in environments (e.g., solid metal oxide particles). The cell membrane of c-type cytochromes promotes the direct electron transfer to GO, and the redox active species produced by the cells function as electron transfer mediators. Both of the direct and indirect pathways are likely involved in the process of extracellular electron transfer (Wang et al., 2011a). Recently, reduction of GO by *Escherichia Coil* was also reported in anaerobic conditions containing glucose, and glycolysis process from metabolic activity of the cells was possibly involved in reduction of GO (Akhavan and Ghaderi, 2012).

3. Preparation of 2D and 3D graphene materials

The flexible 2D structure of graphene materials make them versatile building blocks to construct 2D and 3D macroscopic materials, in which individual nanosheets are connected by virtue of hydrogen bonding, ionic interaction, hydrophobic effects, and/or π-π interactions. The resulting 2D and 3D graphene materials not only retain some key properties of individual graphene sheets, but also develop collective properties resulting from their unique structures (Wu et al., 2012; Xu and Shi, 2011). Of equal importance is that a great number of functional

materials can be incorporated into 2D and 3D graphene materials, improving the performance of pristine graphene materials and extending their applications to new fields.

3.1. Methods to prepare 2D graphene materials

3.1.1. Langmuir-Blodgett method

Langmuir-Blodgett technique, an approach commonly use for depositing nanoparticles and macromolecules on substrates as thin films with controlled thickness (Park and Advincula, 2011; Tao et al., 2008), was also applied to prepare transparent graphene films suitable for optoelectronic applications. Unlike traditional transparent electrodes of ITO and FTO, graphene films were prepared in large scale at low cost, and hold great promise in the development of flexible electronic devices. The electrostatic repulsion between negatively charged GO prevents their overlapping, giving rise to stable GO monolayer film at the interfaces of air and the mixture of water/methanol. The formed GO film can be readily transferred to flat substrates through Langmuir-Blodgett technique (Cote et al., 2009b). Morphologies of GO film evolve from individual sheets to close-packed and wrinkled structures by controlling its density during deposition (Zheng et al., 2011). It is much more challenging to prepare rGO films with higher conductivity, because of the limited colloidal stability of rGO in organic solvents. After modification of rGO with surfactant, stable dispersion of rGO in 1,2-dichloroethane was obtained. Transparent and conducting film was then prepared through Langmuir-Blodgett technique from the solution of rGO in water and 1,2-dichloroethane (Li et al., 2008b).

3.1.2. Layer-by-layer assembly

Layer-by-layer technique has been widely adopted for fabricating multilayer films with tunable composition and architectures. The driving forces involved in layer-by-layer assembly

generally include electrostatic interactions, hydrogen bonding, and covalent bonding. Based on electrostatic interactions between different charged species, multilayer films of CNTs and rGO have been fabricated from rGO with negatively charged surfaces and amine-functionalized CNTs with positively charged surfaces (Byon et al., 2011). Similarly, rGO carrying positive charge imparted by poly(ethyleneimine) coating can also be assembled with acid treated CNTs with negatively charged surface into hybrid films (Fig. 4) (Yu and Dai, 2010). CNTs incorporated into the hybrid films function as spacers to avoid aggregation of rGO caused by the strong π-π interactions between their basal planes. The layer-by-layer technique was also extended to prepare multilayer films of negatively charged rGO and inorganic nanoparticles (Li et al., 2011c). A example of multilayer films relying on hydrogen bonding was built upon from rGO and poly(vinyl alcohol) (Zhao et al., 2010).

(Figure 4 is here)

3.1.3. Electrochemical deposition

Electrophoretic deposition is a technique to deposit thin films through electrical field driven movement of charged colloidal particles towards the electrodes with opposite charges (Van der Biest and Vandeperre, 1999). This method is easy to scale-up and suitable to a wide range of inorganic, polymer, and composite colloidal particles (Chavez-Valdez et al., 2013), leading to precisely controlled film thickness and excellent uniformity at high deposition rates. The charged surfaces of GO and rGO enables the direct electrophoretic deposition of their films. By applying a positive potential of 10 V, the negatively charged GO moves towards the positive electrode and form a uniform film within 10 min. Oxygen functionalities were eliminated in the process possibly because of reactions including oxidation of carboxylate, oxidative decarboxylation, and

dimerization of radicals. And consequently, the electrophoretic deposited GO film exhibits two fold increase of electrical conductivity compared with that prepared by filtration method (An et al., 2010). The composition and properties of solution affects the structure of deposited graphene films, as evidenced by porous graphene film obtained by introducing charging and dispersing additive to the solutions (Ata et al., 2012).

Electrophoretic deposition is not restricted to two-dimensional substrates, as manifested by the successful deposition of rGO on three-dimensional nickel foam (Chen et al., 2010), and can be extended to prepare graphene composite films. Hybrid films with different contents of rGO and CNTs were obtained from solutions with different ratios of the two components (Zhu et al., 2011b). Multilayer films of rGO and quantum dots were prepared by repeated deposition of rGO and quantum dots on flat substrates (Guo et al., 2010). An example of direct deposition of chemically modified graphene with controlled functionalities was transparent films of MoS_2-rGO (Lin et al., 2013).

One important finding is that electrodeposition and electrochemical reduction of GO can be achieved simultaneously on conducting substrates through employing negative potentials around -1.0 or -1.2 V, or repeated cyclic voltammetry (CV) with the lower potential of about -1.2 V in solutions with pH from 1.5 to 12.5 (Chen et al., 2011b). The conductivity of GO dispersion, adjustable by adding different amounts of electrolytes, is a crucial factor affecting the deposition process. The suitable conductivity was in the range of 4 to 25 mS cm^{-1}. No detectable deposition occurred, if conductivity of the solution was too low. When the conductivity was higher than 25 mS cm^{-1}, GO dispersion became unstable (Hilder et al., 2011). As an extension of the one-step technique, composite films of rGO and metal nanoparticles with a sandwiched structure was successfully prepared from mixtures of GO and metal ion salts under cathodic conditions (Liu et

al., 2011). By changing higher and lower potentials in CV scans, electrochemical reduction of GO and polymerization of monomers occurs independently at different potential ranges, leading to the formation of hybrid films of rGO and conducting polymers with multilayer structures. The top layer can be adjusted as conducting polymers or rGO by varying the directions of CV scans (Fig. 5) (Tang et al., 2012).

(Figure 5 is here)

3.1.4. Vacuum filtration

Vacuum filtration, traditionally used to prepare paper-like films from inorganic nanomaterials with platelet morphology, such as vermiculite and mica (Ballard and Rideal, 1983), was first applied to prepare free-standing graphene paper by filtrating aqueous dispersion of GO through a porous membrane filter in 2007 (Dikin et al., 2007). The thickness of GO paper can be adjusted by changing the volume or concentration of the dispersion. This kind of paper is usually characterized by multilayer structures, because graphene sheets tend to be spontaneously arranged in a sheet-by-sheet manner at the liquid-solid interface (Fig. 6) (Yang et al., 2011). After annealing at 220 °C, Young's modulus of graphene paper increased from ~20 GPa to 41.8 GPa, as tensile strength increased from ~150 MPa to 293.3 MPa. The mechanical performance of graphene paper outperforms other inorganic paper-like materials such as graphite foils, and the conductivity of graphene paper treated at 500 °C reaches 351 S m^{-1} (Chen et al., 2008).

(Figure 6 is here)

Taking advantages of the colloid nature of graphene and the well-established methods for synthesizing various metal, metal oxide or polymer colloidal nanostructures, vacuum filtration opens the possibility for screening composite materials with desired functionalities introduced

into graphene paper. In order to improve biocompatibility, Tween 20 was introduced to prepare graphene paper with no cytotoxicity to mammalian cells, leading the way for biocompatible graphene paper (Park et al., 2010). Aiming at improving electrochemical performances, polyaniline (PANI) nanofibers were uniformly sandwiched between rGO sheets to produce composite graphene paper (Wu et al., 2010). Composite graphene paper of rGO functionalized with metal oxide nanoparticles (e.g., SnO_2, NiO, MnO_2, and SiO_2) can be prepared in a similar way (Li et al., 2011b; Wang et al., 2010a).

3.1.5. Solvent evaporation

It was initially found that GO can be assembled into film at air-liquid interface by simply heating its solution at 80 °C for about 40 min. The size and thickness of the film is determined respectively by surface area of the interface and heating time (Chen et al., 2009). Another work revealed that chemical reduction and self-assembly of GO at the interface can be achieved simultaneously if GO solution containing hydrazine was heated (Zhu et al., 2009). The air-liquid interface provides an ideal platform for hybridizing graphene with other components, leading to composite films with an identical composition to that in solutions (Shao et al., 2012). However, the films at air-liquid interface must be transferred to substrates, and handled carefully to retain structural integrity of the films. We found that if water was completely removed, GO membrane deposited on PTFE substrates can be easily peeled off (Xiao et al., 2013). This strategy was also adopted to prepare rGO paper by adding reducing reagent of hydrogen iodine to GO solution (Cong et al., 2013). However, the mechanical properties of graphene paper prepared by solvent-evaporation are usually poorer relative to that obtained from vacuum filtration.

3.2. Methods to prepare 3D graphene materials

3.2.1. Hydrothermal reduction

The first example of 3D graphene materials, i.e., graphene hydrogel, was prepared by hydrothermal treatments of GO dispersions at a concentration not lower than 2 mg mL^{-1} at 180 °C for 12 h (Xu et al., 2010b). After freeze-dried, electrical conductivity of the prepared graphene hydrogel can reach 5×10^{-3} S cm^{-1}, and the modulus is as high as 450-490 kPa. The mechanism of forming graphene hydrogel was proposed as follows: Before hydrothermal reduction, the hydrophilic GO sheets are well dispersed in water; with increasing the reduction time, the oxygen functionalities on GO are eliminated gradually, and the conjugated structures are restored; the growing hydrophobic and π-π interactions between rGO lead to random self-assembly of the flexible sheets in 3D, which eventually form hydrogel with pore size distribution from sub-micrometer to a few micrometers (Zhang and Shi, 2011). If the concentration of GO is lower than 2 mg mL^{-1}, the partial overlapping and crosslinking is more difficult to take place between rGO sheets, and only dispersions or aggregated powders can be obtained. In addition, hydrothermal method requires high temperature and long reaction time to form stable graphene hydrogel.

3.2.2. Chemical reduction

The presence of reducing reagents, including sodium ascorbate, ascorbic acid, hydroiodic acid, sulfur-containing chemicals, and hydroquinone (Chen and Yan, 2011; Sheng et al., 2011), can promote the reduction and self-assembly of GO into graphene hydrogel under mild condition (~ 95 °C) in a shorter reaction time (within 1.5 h). A combination of functionalization, lyophilization, and microwave treatment was employed to prepare ultralight graphene hydrogel

in which GO was first functionalized and assembled into graphene hydrogel in aqueous solutions containing a weak reducing reagent, i.e., ethylenediamine, and microwave irradiation was then applied to eliminate oxygen functional groups (Hu et al., 2013).

The properties of graphene hydrogel can be easily tuned by introducing different functionalities in chemical reduction and self-assembly process, for example, polymers, CNTs, and metal nanoparticles (Hu et al., 2012; Qiu et al., 2010; Sui et al., 2012). Taking the advantages of the fascinating properties of dopamine, e.g., reducing activity, self-polymerization, and strong adhesion of polydopamine to solid substrates, simultaneous reduction of GO and coating of polydopamine was achieved to produce graphene hydrogel functionalized with polydopamine (Gao et al., 2013). Iron oxide nanoparticles were immobilized on graphene hydrogel through one-step reduction using Fe(II). The composition and morphology of iron oxide nanoparticles can be controlled by adjusting pH of the solutions (Fig. 7) (Cong et al., 2012).

(Figure 7 is here)

3.2.3. Template-directed method

Template-directed method provides an approach to fabricating 3D graphene materials with well-controlled pore size distributions. The commonly used sacrificial templates, i.e., polystyrene (PS) and silica colloidal particles, have been applied to prepare 3D graphene materials. A mixture of PS and GO was filtrated through a membrane. Dissolution of PS particles by toluene resulted in graphene foam with uniform pore structures (Fig. 8) (Choi et al., 2012). Capillary modeling, a more general approach to wrap GO sheets on template particles, was achieved in a device for aerosol spray pyrolysis, leading to uniform hollow rGO capsules

(Sohn et al., 2012). The template method was also extended to prepare nitrogen and sulfur doped porous graphene by impregnating solutions containing GO, poly(vinyl pyrrolidone) and sulfonated PS particles onto nickel foam, followed by freeze-drying and calcination in nitrogen atmosphere to remove the template and PVP surfactants (Wang et al., 2013d).

(Figure 8 is here)

However, the pore size of graphene foam templated by PS is limited to micrometers due to the relatively larger size of template particles (20 μm). Methyl functionalized silica nanoparticles (30 to 120 nm) were developed as templates to prepare nanoporous graphene foam (Huang et al., 2012). Core-shell structure of GO wrapped onto silica nanoparticles was prepared by virtue of hydrophobic interaction between amphiphilic GO and methyl groups on silica templates (Kim et al., 2010b). Centrifugation was then applied to condense the nanoparticles, followed by HF etching of silica templates.

3.2.4. Chemical vapor deposition

Chemical vapor deposition (CVD) can produce graphene materials with higher electrical conductivity and fewer defects than that prepared from wet-chemical approaches. Methane was first employed as the carbon precursor to synthesize 3D graphene materials by CVD, using porous nickel foam with 3D interconnected channels as substrate. The resulting graphene foam is monolithic with 3D interconnected graphene sheets, and its density is as low as 5 mg cm^{-3}, which is comparable to the lightest aerogel (2-3 mg cm^{-3}) (Chen et al., 2011c). Afterwards, a study revealed that graphene foam exhibiting almost the same morphology can be produced using safer and cheaper carbon precursors such as ethanol (Cao et al., 2011). With ethanol as the precursor, graphene foam coated with a dense layer of CNTs mesh was prepared via a two-step CVD

method (Dong et al., 2012a). The monolithic graphene foam with high surface areas and excellent electrical conductivity is a promising candidate for a wide spectrum of applications (Dong et al., 2012b; Maiyalagan et al., 2012; Yong et al., 2012).

4. Bioelectrochemical applications of 2D and 3D graphene materials

The self-assembled 2D and 3D graphene materials, functionalized with metal nanoparticles, polymers and biomolecules, are promising candidates for bioelectrochemical applications, especially in the fields of electrochemical biosensors and biological fuel cells. Electrochemical biosensors with high sensitivity have found widespread uses in clinic diagnosis, environment monitoring, and quality controls in industrial, food, and agricultural products (Ronkainen et al., 2010). Biological fuel cells represent an important kind of electrochemical energy conversion devices that can directly transform chemical energy from biomass into electrical energy with high efficiency and low or zero emission of pollutants. The biological fuel cells also have the ability to integrate environmental bioremediation with power production (Logan, 2009).

4.1. Electrochemical biosensors

4.1.1. 2D graphene materials for electrochemical biosensors

Real-time and point-of-care detection necessitates the development of portable and wearable medical devices, in which flexible electrodes are the crucial components (Windmiller and Wang, 2013). Graphene paper is a promising scaffold to construct flexible electrodes because of its unique properties, such as high mechanical strength, structural uniformity, and excellent electrical conductivity. A hybrid film was prepared by filtration of Nafion functionalized rGO, and then modified by organophosphorous hydrolase (OPH). The remarkable electrical conductivity of rGO and low interfacial resistance of Nafion empowered OPH-modified

graphene film with excellent electrochemical performance towards detection of organophosphate with a sensitivity of 10.7 nA μM^{-1} and detection limit of 0.137 μM. Importantly, after 100 binding cycles, the sensitivity of the flexible biosensor was still as high as 9.7 nA μM^{-1} (Choi et al., 2010). In order to achieve real-time detection of biomolecules released from living cells, RGD-peptide, which can facilitate the attachment and growth of cells, was covalently modified onto graphene paper. This flexible electrode was further employed for monitoring of nitric oxide released from endothelial cells, while keeping its original performance after 45 times of bending and relaxing cycles (Guo et al., 2012).

Because of the lack of surface functionalities, it is challenging to modify graphene paper with high density nanoparticles. A combined approach of 2D assembly of gold nanoparticles at oil-water interface coupled with dip-coating method was employed to prepare freestanding graphene paper electrodes covered by closely packed gold nanoparticles. The electrode exhibited excellent electrochemical performance for electro-oxidation of glucose, and superior biocompatibility, and allowed for direct detection of low concentration H_2O_2 secreted by living cells (Fig. 9) (Xiao et al., 2012b). Another advantage of this modular approach is the feasibility to tune the size, composition and morphology of the active nanoparticles. In a follow-up work, core-shell Au@Pt nanoparticles were successfully coated on graphene paper, and applied for the detection of nitric oxide released by living cells under oxidative stress (Zan et al., 2013). In order to increase surface areas of graphene paper, it was first modified by electrodeposition of MnO_2 nanowires, which provide more growing sites for metallic nanoparticles. The constructed electrode was successfully applied for detection of H_2O_2 from living cell with a variation of amperometric response less than 5% after 100 repeated bending (Xiao et al., 2012a).

(Figure 9 is here)

4.1.2. 3D graphene materials for electrochemical biosensors

In comparison with 2D graphene paper, it is possible to introduce more enzymes and catalysts into 3D graphene materials because of increased surface areas. Prussian blue modified graphene hydrogel was prepared by adding $FeCl_3$ solution containing ascorbic acid into the mixture of GO and ferricyanide. The detection limit of the prepared electrode for H_2O_2 was as low as 5 nM (Chen et al., 2012b). Co_3O_4 nanowires were uniformly deposited onto CVD-grown 3D graphene foam through hydrothermal method, and used as free-standing electrodes towards the analysis of glucose, affording a detection limit of 25 nM (Dong et al., 2012b). Graphene foam functionalized with nickel was prepared by annealing lithographically defined 3D porous carbon coated nickel at 750 °C for 20 min under the flow of forming gas containing 5% H_2 and 95% N_2 (Fig. 10) (Xiao et al., 2012c). The electrode exhibits a good linear range for glucose concentration from 1 to 10 mM (Xiao et al., 2012d). A variety of noble metal nanoparticles, including Pt, Au and Pd were further electrodeposited onto the 3D graphene foam prepared by lithographic method. The onset potential for H_2O_2 reduction appeared at 0.1 V while the reduction peak was observed at -0.1 V on Pd nanoparticles modified graphene foam (Sattayasamitsathit et al., 2013).

(Figure 10 is here)

4.2. Biological fuel cells

4.2.1. 2D graphene materials for biological fuel cells

Among the different types of fuel cells, biological fuel cells are distinguished from the others by utilizing biocatalysts, i.e., complete living cells, organelles, and enzymes, as the anode

or cathode to generate electrical power from biomass or biofuels (Cooney et al., 2008). The electron transfer efficiency between biocatalysts and electrodes directly determines bioelectrocatalytic process and performance of biological fuel cells (Logan et al., 2007). A collection of intriguing properties such as high surface areas, excellent biocompatibility and high electrical conductivity enabled the use of graphene-based materials in *E. coli* catalyzed microbial fuel cells. The attachment of bacteria onto the stainless steel mesh anode was enhanced by graphene, and the power density was improved by 17 to 18 times compared with bare stainless steel mesh electrode or the one modified with polytetrafluoroethylene (Zhang et al., 2011). To further enhance the interaction of negatively charged bacteria with graphene film coated on carbon paper, a positively charged layer of poly(3,4-ethylenedioxythiophene) (PEDOT) was deposited on the graphene film by electropolymerization. The short-circuit current achieved by the microbial fuel cell based on graphene/PEDOT anode was 3.59 A m^{-2}, which is almost 7 times higher than that achieved by carbon paper electrode. The maximum power output reached 873 mW m^{-2} on the graphene/PEDOT electrode, representing a 15-fold increase relative to the result from carbon paper bioanodes (Wang et al., 2013c).

The application of 2D graphene film in enzymatic biofuel cells was also demonstrated in multilayer electrodes. When graphene was used as spacer, the multilayer films of multiwalled carbon nanotubes or methylene green were readily assembled onto electrodes through layer-by-layer strategy based on electrostatic and/or π-π interactions (Wang et al., 2011b). The biocatalyst of glucose dehydrogenase was then dip-coated on the multilayer film to prepare bioanodes. The layer-by-layer strategy enables the formation of structurally uniform multilayer film, and the coverage of graphene was increased upon repeating assembly processes. In couple with laccase-based biocathode, the assembled glucose/oxygen biofuel cell exhibits an open-circuit voltage of

0.69 V and a maximum power density of 22.50 μW cm^{-2} at 0.48 V in phosphate buffer solution containing 10 mM NAD^+ and 30 mM glucose (Fig. 11).

(Figure 11 is here)

4.2.2. 3D graphene materials for biological fuel cells

3D graphene materials with increased surface areas for bacterial colonization or biocatalysts immobilization are emerging as new electrode substrates for biological fuel cells. In order to increase electrical conductivity of graphene sponge, stainless-steel current collectors were incorporated into 3D graphene material. The maximum power density produced by the composite anode was 14 times of that produced by graphene-sponge anode. And importantly, the cost was estimated to be at least one order of magnitude less than commercial graphite electrode (Xie et al., 2012). A feasible deposition method was developed to prepare 3D rGO-nickel foam anode for microbial fuel cells, in which the loading amount of rGO and electrode surface areas were controlled by the number of rGO loading cycles. The uniform macroporous scaffold enables effective mass diffusion of the culture medium, and provides large accessible surface area for microbial colonization. Furthermore, the controlled deposition method was suitable for fabricating large-scale electrodes. At steady state of power generation, the microbial fuel cells with rGO-nickel foam produced a substantially higher power density than that of nickel foam and other conventional carbon based electrode. The optimal volumetric power density reached 661 W m^{-3} based on the volume of the anode material, or 27 W m^3 based on the volume of the anode chamber (Wang et al., 2013a).

Free-standing 3D graphene electrode made it possible to develop light-weight devices with high performance. Ice segregation induced self-assembly, a freeze casting technique towards the

preparation of macroporous materials with aligned structures (Vickery et al., 2009), was applied to prepare 3D chitosan/vacuum-stripped graphene (CHI/VSG) scaffold with hierarchically porous structures. The prepared macroporous material can facilitate colonization of bacteria in the scaffold interior and enhance the contact of biocompatible VSG and bacteria, and the meso-micropores increase the available surface area of graphene for electron transfer (Fig. 12). The synergistic effect of hierarchical pores in the anode significantly improved the performance of microbial fuel cells, leading to a maximum power density of 1530 mW m^{-2}, which is 78 times higher than that based on carbon cloth anode (19.5 mW m^{-2}) (He et al., 2012). In order to overcome the unfavorable adhesion of bacteria on hydrophobic graphene sheets, hydrophilic PANI was electrodeposited on monolithic graphene foam, resulting in a confluent biofilm of *Shewanella oneidensis* on graphene surface. The bacteria also densely adhered on graphene surface deep inside the 3D electrode, whereas only some of outmost surface was coated by biofilm on 3D graphene without PANI functionalization. The maximum power density obtained from the microbial fuel cell based on 3D graphene/PANI is ~768 mW m^{-2}, which is about 4 times higher than that from carbon cloth (~158 mW m^{-2}) (Yong et al., 2012).

(Figure 12 is here)

5. Conclusions and perspectives

The flexible structures and tunable functionalities make graphene sheets an attractive type of building blocks for 2D and 3D materials. A number of approaches have been developed to fabricate these materials, which not only preserve the inherent properties of individual graphene sheets, but also develop additional functions arising from their hierarchical structures. Despite the considerable achievements in this area during the last a few years, their successful implementation into practical applications will require further research efforts from different

areas combining multiple disciplines including chemistry, physics, engineering, material and biological science.

The research on hierarchical structures based on graphene sheets is still in its infancy, with key issues to be addressed in future studies. First, increasing evidence has demonstrated that the structures and properties of 2D and 3D graphene architectures is highly dependent on those of the building blocks. However, it is still challenging to synthesize monodisperse graphene sheets with controlled sizes, shapes and functionalities. Second, the electrical conductivity is a crucial factor that determines the performances of graphene materials. Nonetheless, there is still a lack of approaches to efficiently restore the aromatic framework to produce graphene sheets with low oxygen to carbon ratios. Third, the relationships between the structures and properties of the hierarchical graphene materials have still not been fully understood, and consequently it is desired to explore guidelines for rational design and synthesis of these materials. Finally, the application of 2D and 3D graphene materials is not limited to the above-mentioned research areas, and it is possible to introduce novel functional building blocks into 2D and 3D graphene materials with enhanced performance in other fields through the existing and newly-developed methods.

Acknowledgements

H.D. thanks the program of Nanyang Assistant Professorship and the Arkray-NTU joint research project for financial support. H.G. is a recipient of graduate research scholarship supported by Nanyang Technological University, Singapore.

References

Akhavan, O., Ghaderi, E., 2012. Carbon 50 (5), 1853-1860.

An, S.J., Zhu, Y.W., Lee, S.H., Stoller, M.D., Emilsson, T., Park, S., Velamakanni, A., An, J.H., Ruoff, R.S., 2010. J. Phys. Chem. Lett. 1 (8), 1259-1263.
Ata, M.S., Sun, Y., Li, X., Zhitomirsky, I., 2012. Colloid Surf. A: Physicochem. Eng. Asp. 398, 9-16.
Bai, H., Li, C., Shi, G.Q., 2011. Adv. Mater. 23 (9), 1089-1115.
Ballard, D.G.H., Rideal, G.R., 1983. J. Mater. Sci. 18 (2), 545-561.
Bi, H.C., Xie, X., Yin, K.B., Zhou, Y.L., Wan, S., He, L.B., Xu, F., Banhart, F., Sun, L.T., Ruoff, R.S., 2012. Adv. Funct. Mater. 22 (21), 4421-4425.
Brodie, B.C., 1859. Phil. Trans. R. Soc. Lond. 149, 249-259.
Byon, H.R., Lee, S.W., Chen, S., Hammond, P.T., Shao-Horn, Y., 2011. Carbon 49 (2), 457-467.
Cao, X.H., Shi, Y.M., Shi, W.H., Lu, G., Huang, X., Yan, Q.Y., Zhang, Q.C., Zhang, H., 2011. Small 7 (22), 3163-3168.
Chavez-Valdez, A., Shaffer, M.S.P., Boccaccini, A.R., 2013. J. Phys. Chem. B 117 (6), 1502-1515.
Chen, C.M., Yang, Q.H., Yang, Y.G., Lv, W., Wen, Y.F., Hou, P.X., Wang, M.Z., Cheng, H.M., 2009. Adv. Mater. 21 (29), 3007-3011.
Chen, D., Feng, H.B., Li, J.H., 2012a. Chem. Rev. 112 (11), 6027-6053.
Chen, D.Z., Li, L.D., Guo, L., 2011a. Nanotechnology 22 (32), 325601.
Chen, H., Muller, M.B., Gilmore, K.J., Wallace, G.G., Li, D., 2008. Adv. Mater. 20 (18), 3557-3561.
Chen, J., Li, C., Shi, G.Q., 2013. J. Phys. Chem. Lett. 4 (8), 1244-1253.
Chen, L., Wang, X.J., Zhang, X.T., Zhang, H.M., 2012b. J. Mater. Chem. 22 (41), 22090-22096.
Chen, L.Y., Tang, Y.H., Wang, K., Liu, C.B., Luo, S.L., 2011b. Electrochem. Commun. 13 (2), 133-137.
Chen, W.F., Yan, L.F., 2011. Nanoscale 3 (8), 3132-3137.
Chen, Y., Zhang, X., Yu, P., Ma, Y.W., 2010. J. Power Sources 195 (9), 3031-3035.
Chen, Z., Yu, D.S., Xiong, W., Liu, P.P., Liu, Y., Dai, L.M., 2014. Langmuir 30 (12), 3567-3571.
Chen, Z.P., Ren, W.C., Gao, L.B., Liu, B.L., Pei, S.F., Cheng, H.M., 2011c. Nature Mater. 10 (6), 424-428.
Cheng, C., Li, D., 2013. Adv. Mater. 25 (1), 13-30.
Choi, B.G., Park, H., Park, T.J., Yang, M.H., Kim, J.S., Jang, S.Y., Heo, N.S., Lee, S.Y., Kong, J., Hong, W.H., 2010. ACS Nano 4 (5), 2910-2918.
Choi, B.G., Yang, M., Hong, W.H., Choi, J.W., Huh, Y.S., 2012. ACS Nano 6 (5), 4020-4028.
Compton, O.C., Nguyen, S.T., 2010. Small 6 (6), 711-723.
Cong, H.P., Ren, X.C., Wang, P., Yu, S.H., 2012. ACS Nano 6 (3), 2693-2703.
Cong, H.P., Ren, X.C., Wang, P., Yu, S.H., 2013. Energy Environ. Sci. 6 (4), 1185-1191.
Cooney, M.J., Svoboda, V., Lau, C., Martin, G., Minteer, S.D., 2008. Energy Environ. Sci. 1 (3), 320-337.
Cote, L.J., Cruz-Silva, R., Huang, J.X., 2009a. J. Am. Chem. Soc. 131 (31), 11027-11032.
Cote, L.J., Kim, F., Huang, J.X., 2009b. J. Am. Chem. Soc. 131 (3), 1043-1049.
Dikin, D.A., Stankovich, S., Zimney, E.J., Piner, R.D., Dommett, G.H.B., Evmenenko, G., Nguyen, S.T., Ruoff, R.S., 2007. Nature 448 (7152), 457-460.
Dong, X.C., Ma, Y.W., Zhu, G.Y., Huang, Y.X., Wang, J., Chan-Park, M.B., Wang, L.H., Huang, W., Chen, P., 2012a. J. Mater. Chem. 22 (33), 17044-17048.
Dong, X.C., Xu, H., Wang, X.W., Huang, Y.X., Chan-Park, M.B., Zhang, H., Wang, L.H., Huang, W., Chen, P., 2012b. ACS Nano 6 (4), 3206-3213.

Dreyer, D.R., Park, S., Bielawski, C.W., Ruoff, R.S., 2010. Chem. Soc. Rev. 39 (1), 228-240.
Fan, Z.J., Kai, W., Yan, J., Wei, T., Zhi, L.J., Feng, J., Ren, Y.M., Song, L.P., Wei, F., 2010a. ACS Nano 5 (1), 191-198.
Fan, Z.J., Wang, K., Wei, T., Yan, J., Song, L.P., Shao, B., 2010b. Carbon 48 (5), 1686-1689.
Fernandez-Merino, M.J., Guardia, L., Paredes, J.I., Villar-Rodil, S., Solis-Fernandez, P., Martinez-Alonso, A., Tascon, J.M.D., 2010. J. Phys. Chem. C 114 (14), 6426-6432.
Gao, H.C., Sun, Y.M., Zhou, J.J., Xu, R., Duan, H.W., 2013. ACS Appl. Mater. Interfaces 5 (2), 425-432.
Gao, H.C., Xiao, F., Ching, C.B., Duan, H.W., 2011. ACS Appl. Mater. Interfaces 3 (8), 3049-3057.
Gao, W., Alemany, L.B., Ci, L.J., Ajayan, P.M., 2009. Nature Chem. 1 (5), 403-408.
Ghosh, S., Calizo, I., Teweldebrhan, D., Pokatilov, E.P., Nika, D.L., Balandin, A.A., Bao, W., Miao, F., Lau, C.N., 2008. Appl. Phys. Lett. 92 (15), 151911.
Guo, C.X., Ng, S.R., Khoo, S.Y., Zheng, X.T., Chen, P., Li, C.M., 2012. ACS Nano 6 (8), 6944-6951.
Guo, C.X., Yang, H.B., Sheng, Z.M., Lu, Z.S., Song, Q.L., Li, C.M., 2010. Angew. Chem., Int. Edit. 49 (17), 3014-3017.
Hassan, H.M.A., Abdelsayed, V., Khder, A., AbouZeid, K.M., Terner, J., El-Shall, M.S., Al-Resayes, S.I., El-Azhary, A.A., 2009. J. Mater. Chem. 19 (23), 3832-3837.
He, Z.M., Liu, J., Qiao, Y., Li, C.M., Tan, T.T.Y., 2012. Nano Lett. 12 (9), 4738-4741.
Hernandez, Y., Nicolosi, V., Lotya, M., Blighe, F.M., Sun, Z.Y., De, S., McGovern, I.T., Holland, B., Byrne, M., Gun'ko, Y.K., Boland, J.J., Niraj, P., Duesberg, G., Krishnamurthy, S., Goodhue, R., Hutchison, J., Scardaci, V., Ferrari, A.C., Coleman, J.N., 2008. Nature Nanotechnol. 3 (9), 563-568.
Hilder, M., Winther-Jensen, B., Li, D., Forsyth, M., MacFarlane, D.R., 2011. Phys. Chem. Chem. Phys. 13 (20), 9187-9193.
Hu, C.G., Cheng, H.H., Zhao, Y., Hu, Y., Liu, Y., Dai, L.M., Qu, L.T., 2012. Adv. Mater. 24 (40), 5493-5498.
Hu, H., Zhao, Z.B., Wan, W.B., Gogotsi, Y., Qiu, J.S., 2013. Adv. Mater. 25 (15), 2219-2223.
Huang, X.D., Qian, K., Yang, J., Zhang, J., Li, L., Yu, C.Z., Zhao, D.Y., 2012. Adv. Mater. 24 (32), 4419-4423.
Hummers, W.S., Offeman, R.E., 1958. J. Am. Chem. Soc. 80 (6), 1339-1339.
Jimenez, P.S.V., 1987. Mater. Res. Bull. 22 (5), 601-608.
Kim, F., Luo, J.Y., Cruz-Silva, R., Cote, L.J., Sohn, K., Huang, J.X., 2010a. Adv. Funct. Mater. 20 (17), 2867-2873.
Kim, J., Cote, L.J., Kim, F., Yuan, W., Shull, K.R., Huang, J.X., 2010b. J. Am. Chem. Soc. 132 (23), 8180-8186.
Krishnan, D., Kim, F., Luo, J.Y., Cruz-Silva, R., Cote, L.J., Jang, H.D., Huang, J.X., 2012. Nano Today 7 (2), 137-152.
Kuila, T., Bose, S., Khanra, P., Mishra, A.K., Kim, N.H., Lee, J.H., 2012. Carbon 50 (3), 914-921.
Lee, C., Wei, X.D., Kysar, J.W., Hone, J., 2008. Science 321 (5887), 385-388.
Lei, Z.B., Lu, L., Zhao, X.S., 2012. Energy Environ. Sci. 5 (4), 6391-6399.
Li, D., Muller, M.B., Gilje, S., Kaner, R.B., Wallace, G.G., 2008a. Nature Nanotechnol. 3 (2), 101-105.

Li, X.L., Zhang, G.Y., Bai, X.D., Sun, X.M., Wang, X.R., Wang, E., Dai, H.J., 2008b. Nature Nanotechnol. 3 (9), 538-542.
Li, Y.G., Wang, H.L., Xie, L.M., Liang, Y.Y., Hong, G.S., Dai, H.J., 2011a. J. Am. Chem. Soc. 133 (19), 7296-7299.
Li, Z.P., Mi, Y.J., Liu, X.H., Liu, S., Yang, S.R., Wang, J.Q., 2011b. J. Mater. Chem. 21 (38), 14706-14711.
Li, Z.P., Wang, J.Q., Liu, X.H., Liu, S., Ou, J.F., Yang, S.R., 2011c. J. Mater. Chem. 21 (10), 3397-3403.
Liang, Y.Y., Li, Y.G., Wang, H.L., Zhou, J.G., Wang, J., Regier, T., Dai, H.J., 2011. Nature Mater. 10 (10), 780-786.
Lin, J.Y., Chan, C.Y., Chou, S.W., 2013. Chem. Commun. 49 (14), 1440-1442.
Liu, C.B., Wang, K., Luo, S.L., Tang, Y.H., Chen, L.Y., 2011. Small 7 (9), 1203-1206.
Logan, B., Cheng, S., Watson, V., Estadt, G., 2007. Environ. Sci. Technol. 41 (9), 3341-3346.
Logan, B.E., 2009. Nat. Rev. Microbiol. 7 (5), 375-381.
Long, D.H., Li, W., Ling, L.C., Miyawaki, J., Mochida, I., Yoon, S.H., 2010. Langmuir 26 (20), 16096-16102.
Low, C.T.J., Walsh, F.C., Chakrabarti, M.H., Hashim, M.A., Hussain, M.A., 2013. Carbon 54, 1-21.
Maiyalagan, T., Dong, X.C., Chen, P., Wang, X., 2012. J. Mater. Chem. 22 (12), 5286-5290.
Marcano, D.C., Kosynkin, D.V., Berlin, J.M., Sinitskii, A., Sun, Z.Z., Slesarev, A., Alemany, L.B., Lu, W., Tour, J.M., 2010. ACS Nano 4 (8), 4806-4814.
Mattevi, C., Kim, H., Chhowalla, M., 2011. J. Mater. Chem. 21 (10), 3324-3334.
Matuyama, E., 1954. J. Phys. Chem. 58 (3), 215-219.
McAllister, M.J., Li, J.L., Adamson, D.H., Schniepp, H.C., Abdala, A.A., Liu, J., Herrera-Alonso, M., Milius, D.L., Car, R., Prud'homme, R.K., Aksay, I.A., 2007. Chem. Mater. 19 (18), 4396-4404.
Mei, X.G., Zheng, H.Q., Ouyang, J.Y., 2012. J. Mater. Chem. 22 (18), 9109-9116.
Nair, R.R., Blake, P., Grigorenko, A.N., Novoselov, K.S., Booth, T.J., Stauber, T., Peres, N.M.R., Geim, A.K., 2008. Science 320 (5881), 1308-1308.
Nethravathi, C., Rajamathi, M., 2008. Carbon 46 (14), 1994-1998.
Novoselov, K.S., Fal'ko, V.I., Colombo, L., Gellert, P.R., Schwab, M.G., Kim, K., 2012. Nature 490 (7419), 192-200.
Novoselov, K.S., Geim, A.K., Morozov, S.V., Jiang, D., Zhang, Y., Dubonos, S.V., Grigorieva, I.V., Firsov, A.A., 2004. Science 306 (5696), 666-669.
Pan, S.Y., Aksay, I.A., 2011. ACS Nano 5 (5), 4073-4083.
Park, J.Y., Advincula, R.C., 2011. Soft Matter 7 (21), 9829-9843.
Park, S., An, J.H., Piner, R.D., Jung, I., Yang, D.X., Velamakanni, A., Nguyen, S.T., Ruoff, R.S., 2008. Chem. Mater. 20 (21), 6592-6594.
Park, S., Mohanty, N., Suk, J.W., Nagaraja, A., An, J.H., Piner, R.D., Cai, W.W., Dreyer, D.R., Berry, V., Ruoff, R.S., 2010. Adv. Mater. 22 (15), 1736-1740.
Park, S., Ruoff, R.S., 2009. Nature Nanotechnol. 4 (4), 217-224.
Pei, S.F., Zhao, J.P., Du, J.H., Ren, W.C., Cheng, H.M., 2010. Carbon 48 (15), 4466-4474.
Pham, T.A., Kim, J.S., Kim, J.S., Jeong, Y.T., 2011. Colloid Surf. A: Physicochem. Eng. Asp. 384 (1-3), 543-548.
Qian, Y., Lu, S.B., Gao, F.L., 2011a. J. Mater. Sci. 46 (10), 3517-3522.
Qian, Y., Lu, S.B., Gao, F.L., 2011b. Mater. Lett. 65 (1), 56-58.

Qiu, L., Yang, X.W., Gou, X.L., Yang, W.R., Ma, Z.F., Wallace, G.G., Li, D., 2010. Chem. Eur. J. 16 (35), 10653-10658.
Ramesha, G.K., Sampath, S., 2009. J. Phys. Chem. C 113 (19), 7985-7989.
Ren, W.C., Cheng, H.M., 2013. Nature 497 (7450), 448-449.
Ronkainen, N.J., Halsall, H.B., Heineman, W.R., 2010. Chem. Soc. Rev. 39 (5), 1747-1763.
Salas, E.C., Sun, Z.Z., Luttge, A., Tour, J.M., 2010. ACS Nano 4 (8), 4852-4856.
Sattayasamitsathit, S., Gu, Y.E., Kaufmann, K., Jia, W.Z., Xiao, X.Y., Rodriguez, M., Minteer, S., Cha, J., Burckel, D.B., Wang, C.M., Polsky, R., Wang, J., 2013. J. Mater. Chem. A 1 (5), 1639-1645.
Schniepp, H.C., Li, J.L., McAllister, M.J., Sai, H., Herrera-Alonso, M., Adamson, D.H., Prud'homme, R.K., Car, R., Saville, D.A., Aksay, I.A., 2006. J. Phys. Chem. B 110 (17), 8535-8539.
Shah, M., Park, A.R., Zhang, K., Park, J.H., Yoo, P.J., 2012. ACS Appl. Mater. Interfaces 4 (8), 3893-3901.
Shao, J.J., Lv, W., Guo, Q.G., Zhang, C., Xu, Q., Yang, Q.H., Kang, F.Y., 2012. Chem. Commun. 48 (31), 3706-3708.
Shao, Y.Y., Wang, J., Engelhard, M., Wang, C.M., Lin, Y.H., 2010a. J. Mater. Chem. 20 (4), 743-748.
Shao, Y.Y., Wang, J., Wu, H., Liu, J., Aksay, I.A., Lin, Y.H., 2010b. Electroanalysis 22 (10), 1027-1036.
Sheng, K.X., Xu, Y.X., Li, C., Shi, G.Q., 2011. New Carbon Mater. 26 (1), 9-15.
Sohn, K., Na, Y.J., Chang, H., Roh, K.M., Jang, H.D., Huang, J.X., 2012. Chem. Commun. 48 (48), 5968-5970.
Stankovich, S., Dikin, D.A., Piner, R.D., Kohlhaas, K.A., Kleinhammes, A., Jia, Y., Wu, Y., Nguyen, S.T., Ruoff, R.S., 2007. Carbon 45 (7), 1558-1565.
Stoller, M.D., Park, S.J., Zhu, Y.W., An, J.H., Ruoff, R.S., 2008. Nano Lett. 8 (10), 3498-3502.
Sui, Z.Y., Meng, Q.H., Zhang, X.T., Ma, R., Cao, B., 2012. J. Mater. Chem. 22 (18), 8767-8771.
Sutter, P.W., Flege, J.I., Sutter, E.A., 2008. Nature Mater. 7 (5), 406-411.
Tang, Y.H., Wu, N., Luo, S.L., Liu, C.B., Wang, K., Chen, L.Y., 2012. Macromol. Rapid Commun. 33 (20), 1780-1786.
Tao, A.R., Huang, J.X., Yang, P.D., 2008. Accounts Chem. Res. 41 (12), 1662-1673.
Van der Biest, O.O., Vandeperre, L.J., 1999. Annu. Rev. Mater. Sci. 29, 327-352.
Vickery, J.L., Patil, A.J., Mann, S., 2009. Adv. Mater. 21 (21), 2180-2184.
Wang, D.H., Kou, R., Choi, D., Yang, Z.G., Nie, Z.M., Li, J., Saraf, L.V., Hu, D.H., Zhang, J.G., Graff, G.L., Liu, J., Pope, M.A., Aksay, I.A., 2010a. ACS Nano 4 (3), 1587-1595.
Wang, G.M., Qian, F., Saltikov, C., Jiao, Y.Q., Li, Y., 2011a. Nano Res. 4 (6), 563-570.
Wang, H.L., Cui, L.F., Yang, Y.A., Casalongue, H.S., Robinson, J.T., Liang, Y.Y., Cui, Y., Dai, H.J., 2010b. J. Am. Chem. Soc. 132 (40), 13978-13980.
Wang, H.Y., Wang, G.M., Ling, Y.C., Qian, F., Song, Y., Lu, X.H., Chen, S.W., Tong, Y.X., Li, Y., 2013a. Nanoscale 5 (21), 10283-10290.
Wang, P., Jiang, T.F., Zhu, C.Z., Zhai, Y.M., Wang, D.J., Dong, S.J., 2010c. Nano Res. 3 (11), 794-799.
Wang, R.H., Wang, Y., Xu, C.H., Sun, J., Gao, L., 2013b. RSC Adv. 3 (4), 1194-1200.
Wang, X., Wang, J.F., Cheng, H.J., Yu, P., Ye, J.S., Mao, L.Q., 2011b. Langmuir 27 (17), 11180-11186.
Wang, Y., Shi, Z.X., Yin, J., 2011c. ACS Appl. Mater. Interfaces 3 (4), 1127-1133.

Wang, Y., Zhao, C.E., Sun, D., Zhang, J.R., Zhu, J.J., 2013c. ChemPlusChem 78 (8), 823-829.
Wang, Z.L., Xu, D., Huang, Y., Wu, Z., Wang, L.M., Zhang, X.B., 2012. Chem. Commun. 48 (7), 976-978.
Wang, Z.L., Xu, D., Wang, H.G., Wu, Z., Zhang, X.B., 2013d. ACS Nano 7 (3), 2422-2430.
Williams, G., Kamat, P.V., 2009. Langmuir 25 (24), 13869-13873.
Williams, G., Seger, B., Kamat, P.V., 2008. ACS Nano 2 (7), 1487-1491.
Windmiller, J.R., Wang, J., 2013. Electroanalysis 25 (1), 29-46.
Wu, D.Q., Zhang, F., Liang, H.W., Feng, X.L., 2012. Chem. Soc. Rev. 41 (18), 6160-6177.
Wu, J.S., Pisula, W., Mullen, K., 2007. Chem. Rev. 107 (3), 718-747.
Wu, Q., Xu, Y.X., Yao, Z.Y., Liu, A.R., Shi, G.Q., 2010. ACS Nano 4 (4), 1963-1970.
Wu, T.S., Liu, S., Luo, Y.L., Lu, W.B., Wang, L., Sun, X.P., 2011. Nanoscale 3 (5), 2142-2144.
Wu, Z.S., Ren, W.C., Gao, L.B., Liu, B.L., Jiang, C.B., Cheng, H.M., 2009a. Carbon 47 (2), 493-499.
Wu, Z.S., Ren, W.C., Gao, L.B., Zhao, J.P., Chen, Z.P., Liu, B.L., Tang, D.M., Yu, B., Jiang, C.B., Cheng, H.M., 2009b. ACS Nano 3 (2), 411-417.
Xiao, F., Li, Y.Q., Gao, H.C., Ge, S.B., Duan, H.W., 2013. Biosens. Bioelectron. 41, 417-423.
Xiao, F., Li, Y.Q., Zan, X.L., Liao, K., Xu, R., Duan, H.W., 2012a. Adv. Funct. Mater. 22 (12), 2487-2494.
Xiao, F., Song, J.B., Gao, H.C., Zan, X.L., Xu, R., Duan, H.W., 2012b. ACS Nano 6 (1), 100-110.
Xiao, X.Y., Beechem, T.E., Brumbach, M.T., Lambert, T.N., Davis, D.J., Michael, J.R., Washburn, C.M., Wang, J., Brozik, S.M., Wheeler, D.R., Burckel, D.B., Polsky, R., 2012c. ACS Nano 6 (4), 3573-3579.
Xiao, X.Y., Michael, J.R., Beechem, T., McDonald, A., Rodriguez, M., Brtunbach, M.T., Lambert, T.N., Washburn, C.M., Wang, J., Brozik, S.M., Wheeler, D.R., Burckel, D.B., Polsky, R., 2012d. J. Mater. Chem. 22 (45), 23749-23754.
Xie, X., Yu, G.H., Liu, N., Bao, Z.N., Criddle, C.S., Cui, Y., 2012. Energy Environ. Sci. 5 (5), 6862-6866.
Xu, L.Q., Yang, W.J., Neoh, K.G., Kang, E.T., Fu, G.D., 2010a. Macromolecules 43 (20), 8336-8339.
Xu, Y.X., Sheng, K.X., Li, C., Shi, G.Q., 2010b. ACS Nano 4 (7), 4324-4330.
Xu, Y.X., Shi, G.Q., 2011. J. Mater. Chem. 21 (10), 3311-3323.
Xue, Y.H., Chen, H., Yu, D.S., Wang, S.Y., Yardeni, M., Dai, Q.B., Guo, M.M., Liu, Y., Lu, F., Qu, J., Dai, L.M., 2011. Chem. Commun. 47 (42), 11689-11691.
Yang, X.W., Qiu, L., Cheng, C., Wu, Y.Z., Ma, Z.F., Li, D., 2011. Angew. Chem., Int. Edit. 50 (32), 7325-7328.
Yong, Y.C., Dong, X.C., Chan-Park, M.B., Song, H., Chen, P., 2012. ACS Nano 6 (3), 2394-2400.
Yoo, J.J., Balakrishnan, K., Huang, J.S., Meunier, V., Sumpter, B.G., Srivastava, A., Conway, M., Reddy, A.L.M., Yu, J., Vajtai, R., Ajayan, P.M., 2011. Nano Lett. 11 (4), 1423-1427.
Yu, D.S., Dai, L.M., 2010. J. Phys. Chem. Lett. 1 (2), 467-470.
Zan, X.L., Fang, Z., Wu, J., Xiao, F., Huo, F.W., Duan, H.W., 2013. Biosens. Bioelectron. 49, 71-78.
Zhang, H.H., Liu, Q., Feng, K., Chen, B., Tung, C.H., Wu, L.Z., 2012. Langmuir 28 (21), 8224-8229.

Zhang, J.L., Yang, H.J., Shen, G.X., Cheng, P., Zhang, J.Y., Guo, S.W., 2010. Chem. Commun. 46 (7), 1112-1114.
Zhang, L., Liang, J.J., Huang, Y., Ma, Y.F., Wang, Y., Chen, Y.S., 2009. Carbon 47 (14), 3365-3368.
Zhang, L., Shi, G.Q., 2011. J. Phys. Chem. C 115 (34), 17206-17212.
Zhang, Y.Z., Mo, G.Q., Li, X.W., Zhang, W.D., Zhang, J.Q., Ye, J.S., Huang, X.D., Yu, C.Z., 2011. J. Power Sources 196 (13), 5402-5407.
Zhao, X., Zhang, Q.H., Hao, Y.P., Li, Y.Z., Fang, Y., Chen, D.J., 2010. Macromolecules 43 (22), 9411-9416.
Zheng, Q.B., Ip, W.H., Lin, X.Y., Yousefi, N., Yeung, K.K., Li, Z.G., Kim, J.K., 2011. ACS Nano 5 (7), 6039-6051.
Zhou, M., Wang, Y.L., Zhai, Y.M., Zhai, J.F., Ren, W., Wang, F.A., Dong, S.J., 2009a. Chem. Eur. J. 15 (25), 6116-6120.
Zhou, Y., Bao, Q.L., Tang, L.A.L., Zhong, Y.L., Loh, K.P., 2009b. Chem. Mater. 21 (13), 2950-2956.
Zhu, C.Z., Guo, S.J., Fang, Y.X., Dong, S.J., 2010a. ACS Nano 4 (4), 2429-2437.
Zhu, C.Z., Guo, S.J., Fang, Y.X., Han, L., Wang, E.K., Dong, S.J., 2011a. Nano Res. 4 (7), 648-657.
Zhu, G., Pan, L.K., Lu, T., Xu, T., Sun, Z., 2011b. J. Mater. Chem. 21 (38), 14869-14875.
Zhu, Y.W., Cai, W.W., Piner, R.D., Velamakanni, A., Ruoff, R.S., 2009. Appl. Phys. Lett. 95 (10), 103104.
Zhu, Y.W., Murali, S., Cai, W.W., Li, X.S., Suk, J.W., Potts, J.R., Ruoff, R.S., 2010b. Adv. Mater. 22 (35), 3906-3924.
Zhu, Y.W., Murali, S., Stoller, M.D., Velamakanni, A., Piner, R.D., Ruoff, R.S., 2010c. Carbon 48 (7), 2118-2122.

Highlights:

Environmentally-friendly strategies to prepare graphene sheets.

Recently developed approaches to fabricate 2D and 3D graphene materials.

The application of 2D and 3D graphene materials in electrochemical biosensors and biological fuel cells.

Graphical abstract

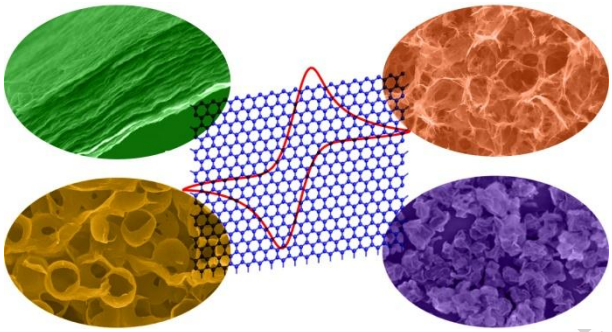

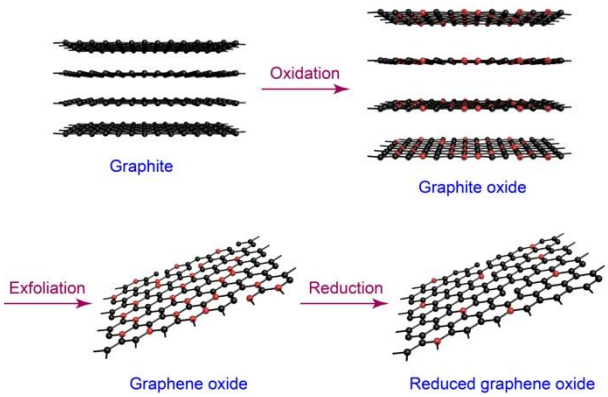

Fig. 1. Schematic illustration of the chemical oxidation, exfoliation, and reduction methods to prepare reduced graphene oxide from graphite.

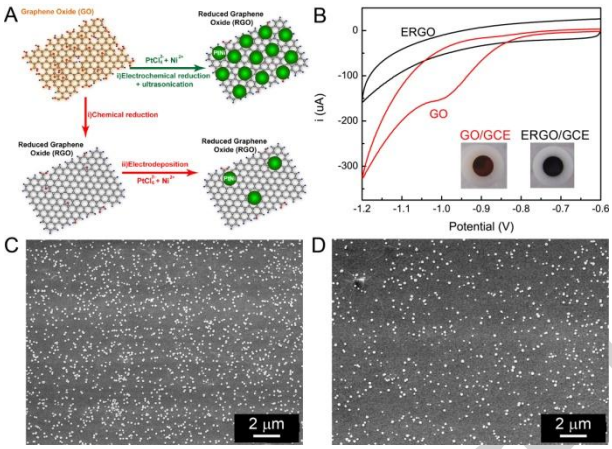

Fig. 2. (A) Schematic illustration of the one-step and two-step methods to prepare PtNi nanoparticles modified rGO film. (B) CV curves and photographs of GO on glass carbon electrodes (GCE) before and after electrochemical reduction. SEM images of PtNi nanoparticles on rGO films prepared through (C) one-step and (D) two-step methods. Reprinted with permission from ref (Gao et al. 2011). Copyright 2011 American Chemical Society.

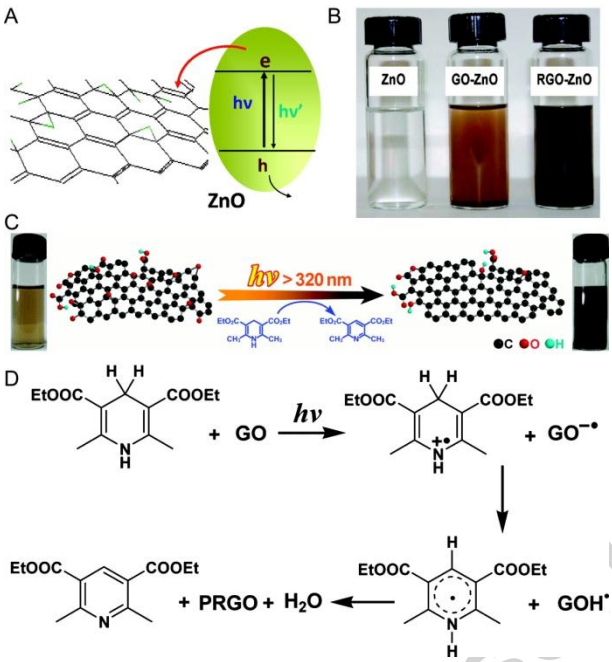

Fig. 3. (A) Reduction mechanism of GO by ZnO under UV excitation. (B) Suspensions of ZnO, GO-ZnO, and RGO-ZnO. Reprinted with permission from ref (Williams and Kamat 2009). Copyright 2009 American Chemical Society. (C) Schematic illustration of photocatalytic reduction of GO by HEH. (D) Proposed chemical reaction mechanism of photochemical reduction of GO by HEH. Reprinted with permission from ref (Zhang et al. 2012). Copyright 2012 American Chemical Society.

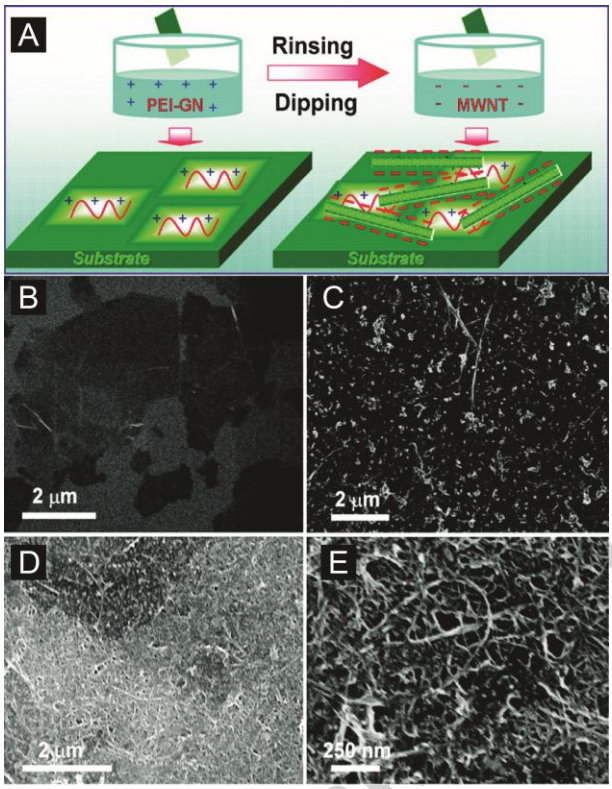

Fig. 4. (A) Schematic illustration of the fabrication process for multi-layer films of positively charged PEI modified grapheme and negatively charged CNTs on substrates. SEM images of (B) the first layer PEI modified graphene, and (C) the first bilayer grapheme and CNTs films deposited on a substrate. (D) and (E) SEM images of the grapheme and CNTs films after ninth deposition cycle under low and high magnifications. Reprinted with permission from ref (Yu and Dai 2010). Copyright 2010 American Chemical Society.

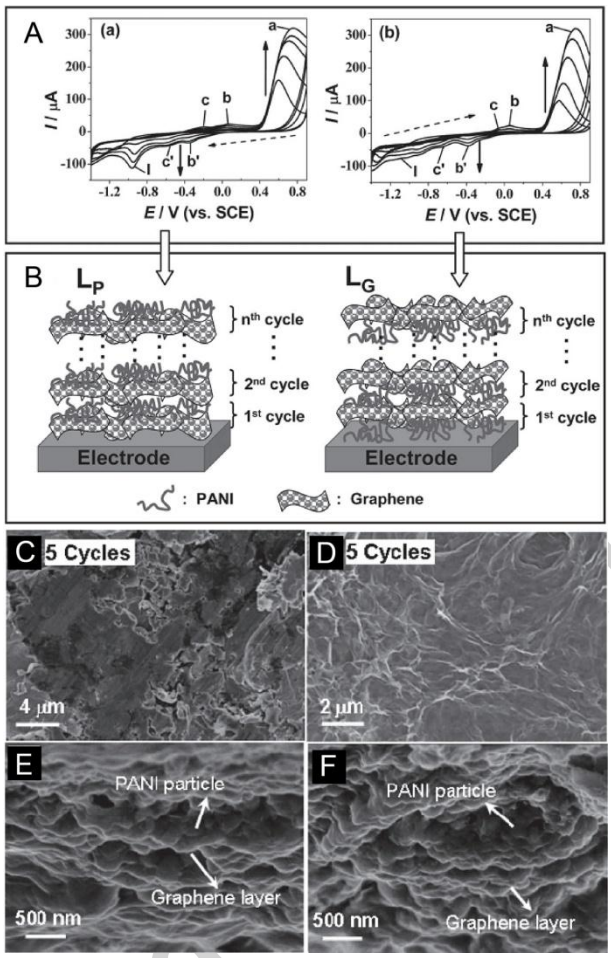

Fig. 5. (A) CV curves of co-electrodeposition of GO and aniline with different initial scan directions as indicated by the dash arrows. (B) Schematic illustration of two structures with PANI (L_P) and graphene (L_G) as the topmost layer. (C and D) Top-view SEM images of the two structures. (E and F) Cross-section SEM images of the two structures. Reprinted with permission from ref (Tang et al. 2012). Copyright 2012 Wiley-VCH Verlag GmbH.

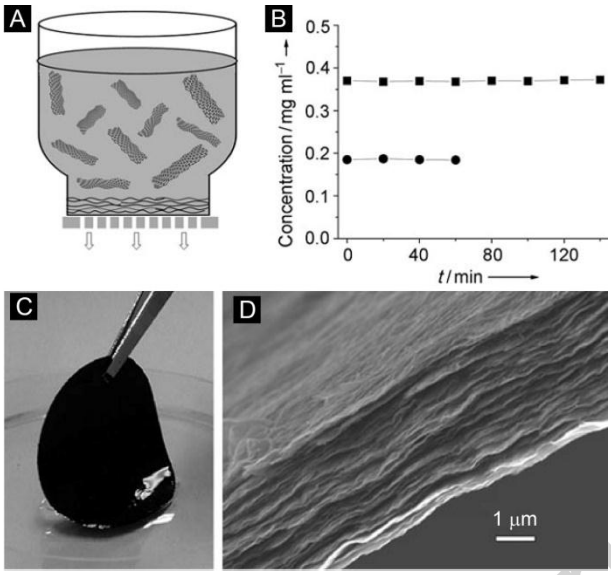

Fig. 6. (A) Schematic illustration of the formation process of graphene paper by filtration method. (B) The concentration of graphene versus filtration time for two samples: (■) 24 mL of 0.37 mg mL^{-1} and (●) 24 mL of 0.18 mg mL^{-1}. (C) Photograph of the as-formed graphene film peeled from the filter membrane. (D) SEM images of the cross-section view of a free-dried graphene paper. Reprinted with permission from ref (Yang et al. 2011). Copyright 2011 Wiley-VCH Verlag GmbH.

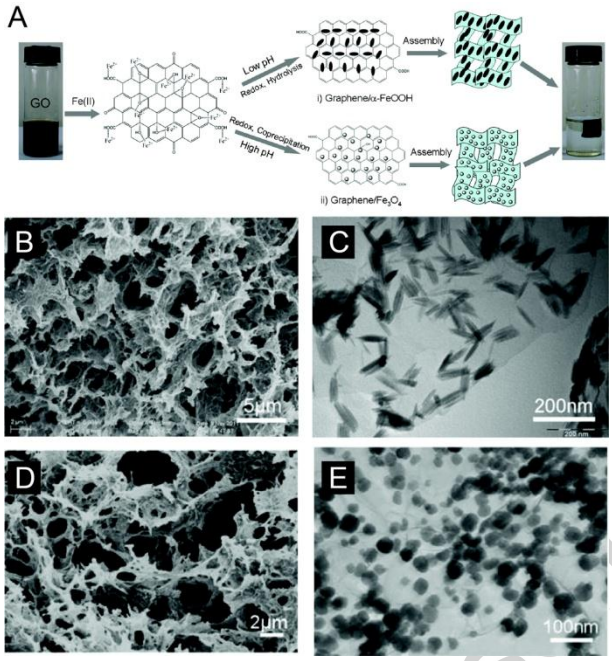

Fig. 7. (A) Schematic illustration of the formation mechanism of rGO and iron oxide nanoparticles with different morphologies. (B) SEM and (C) TEM images of rGO and FeOOH. (D) SEM and (E) TEM images of rGO and Fe_3O_4. Reprinted with permission from ref (Cong et al. 2012). Copyright 2012 American Chemical Society.

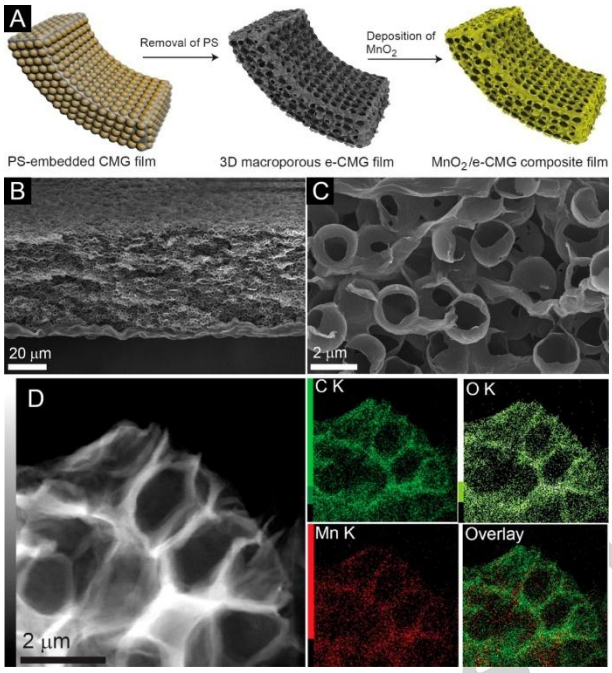

Fig. 8. (A) Schematic illustration of the fabrication process of 3D macroporous graphene films through an embossing process with PS as the templates for embossed chemically modified graphene (e-CMG) film and subsequent deposition of MnO_2 for MnO_2/e-CMG film. (B) Low and (D) high magnified cross-section SEM images of e-CMG films. (D) STEM images and EDS mapping of C, O, Mn, and overlay elements on MnO_2/e-CMG film. Reprinted with permission from ref (Choi et al. 2012). Copyright 2012 American Chemical Society.

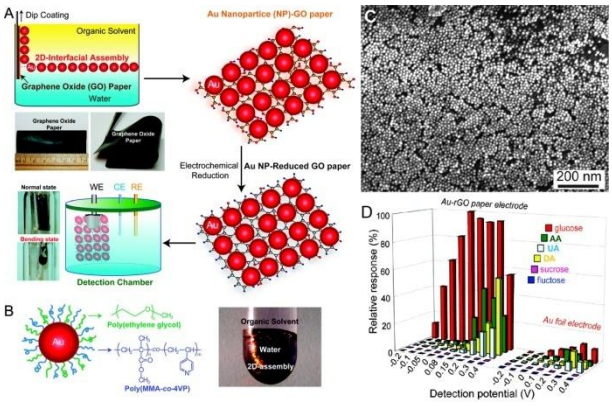

Fig. 9. (A) Schematic illustration of the fabrication process from the 2D assembly Au nanoparticles and graphene paper. (B) Structure of the amphiphilic Au nanoparticles and their assembly at the interface of water and organic solvent. (C) SEM images of 2D assembly of Au nanoparticles on graphene paper. (D) Comparison of the prepared Au nanoparticles-rGO paper electrodes and gold foil towards the detection of different molecules. Reprinted with permission from ref (Xiao et al. 2012b). Copyright 2012 American Chemical Society.

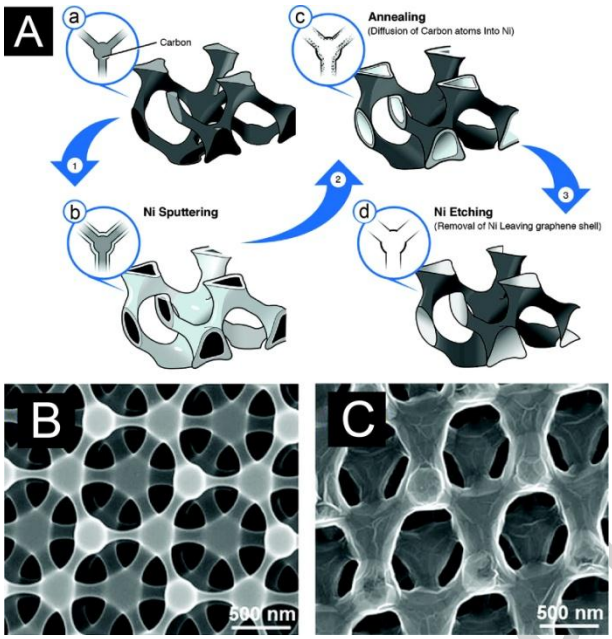

Fig. 10. (A) Schematic illustration of the preparation process and mechanism for chemical conversion of amorphous porous carbon to 3D graphene. (B) SEM images of the prepared 3D graphene. (C) SEM images of the 3D graphene after the modification of Pt nanoparticles. Reprinted from ref (Xiao et al. 2012c). Copyright 2012 American Chemical Society.

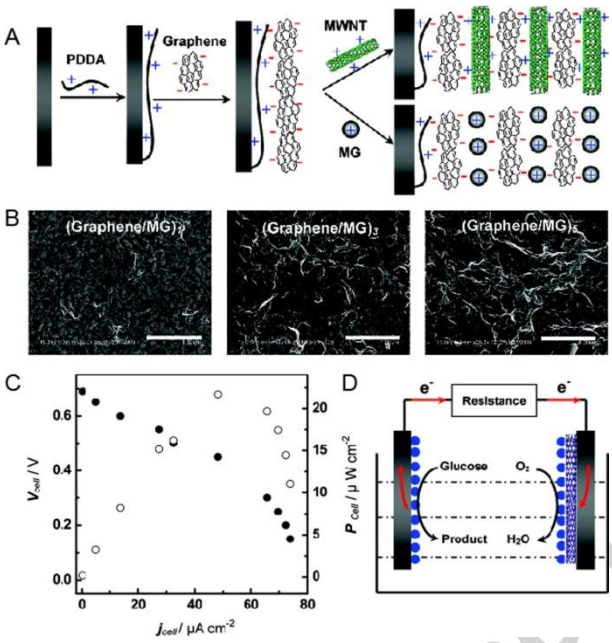

Fig. 11. (A) Schematic illustration of the fabrication process of multi-layered film with graphene as spacer. (B) SEM images of the graphene/methylene green film with different number of layers. (C) Polarization curve of the assembled glucose/oxygen biofuel cell and the dependence of the power output on the current density in the quiescent phosphate buffer containing NAD^+ and glucose under ambient condition. (D) Schematic illustration of the glucose/oxygen biofuels cell. Reprinted with permission from ref (Wang et al. 2011b). Copyright 2012 American Chemical Society.

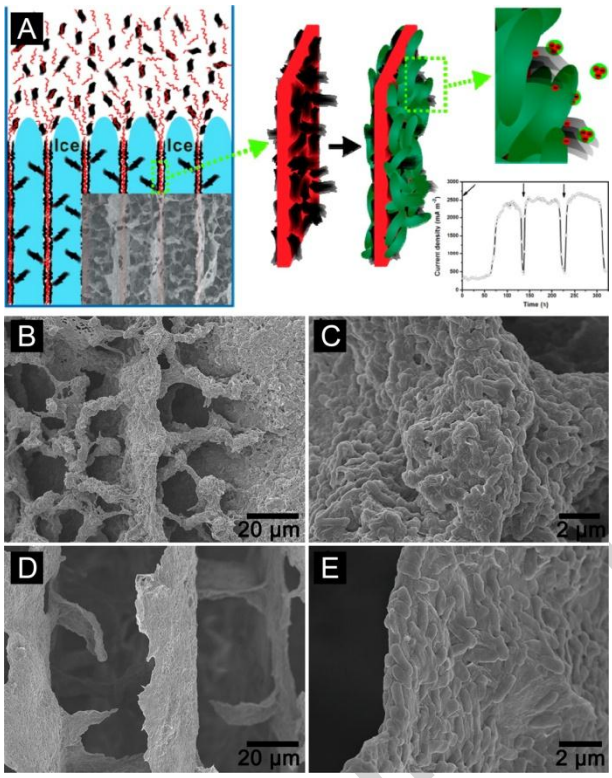

Fig. 12. (A) Schematic illustration of the fabrication process of 3D chitosan/vacuum-stripped grapheme from the ice segregation induced self-assembly. SEM images of (B and C) chitosan/vacuum-stripped grapheme, and (D and E) the scaffolds after incubation with bacteria. Reprinted with permission from ref (He et al. 2012). Copyright 2012 American Chemical Society.